
Article:
Gardner, L.J. orcid.org/0000-0003-3126-2583, Corkhill, C.L. orcid.org/0000-0002-7488-3219, Walling, S.A. et al. (5 more authors) (2021) Early age hydration and application of blended magnesium potassium phosphate cements for reduced corrosion of reactive metals. Cement and Concrete Research, 143. 106375. ISSN 0008-8846

https://doi.org/10.1016/j.cemconres.2021.106375

Cement and Concrete Research 143 (2021) 106375

Contents lists available at ScienceDirect

Cement and Concrete Research

journal homepage: www.elsevier.com/locate/cemconres

Early age hydration and application of blended magnesium potassium phosphate cements for reduced corrosion of reactive metals

Laura J. Gardner [a], Claire L. Corkhill [a], Sam A. Walling [a], James E. Vigor [a], Claire A. Murray [b], Chiu C. Tang [b], John L. Provis [a], Neil C. Hyatt [a,*]

[a] Immobilisation Science Laboratory, Department of Materials Science and Engineering, University of Sheffield, Sheffield S1 3JD, UK
[b] Diamond Light Source, Diamond House, Harwell Science and Innovation Campus, Didcot, Oxfordshire OX11 0DE, UK

ARTICLE INFO

Keywords:
Chemically bonded ceramics (D)
Calorimetry (A)
Hydration (A)
X-ray diffraction (B)
Radioactive waste (E)

ABSTRACT

Magnesium potassium phosphate cements (MKPC) were investigated to determine their efficacy towards retardation of reactive uranium metal corrosion. Optimised low-water content, fly ash (FA) and blast furnace slag (BFS) blended MKPC formulations were developed and their fluidity, hydration behaviour, strength and phase assemblage investigated. In-situ time resolved synchrotron powder X-ray diffraction was used to detail the early age (~60 h) phase assemblage development and hydration kinetics, where the inclusion of BFS was observed to delay the formation of struvite-K by ~14 h compared to FA addition (~2 h). All samples set within this period, suggesting the possible formation of a poorly crystalline binding phase prior to struvite-K crystallisation. Long-term corrosion trials using metallic uranium indicated that MKPC systems are capable of limiting uranium corrosion rates (reduced by half), when compared to a UK nuclear industry grout, which highlights their potential application radioactive waste immobilisation.

1. Introduction

Magnesium potassium phosphate cements (MKPCs) are of growing interest as alternatives to Portland based cements, and are being actively researched for applications such as construction and rapid repairs [1,2], biocements (e.g. dental) [3] and for radioactive waste immobilisation [4–9], particularly for encapsulation of reactive metals (e.g. uranium). These MKPC binders gain their strength via an acid-base reaction between dead-burnt MgO, KH_2PO_4 (KDP) and H_2O to yield struvite-K, $MgKPO_4{\cdot}6H_2O$ (Eq. (1)). This reaction product is an analogue of struvite ($NH_4MgPO_4{\cdot}6H_2O$) [10], which is naturally cementitious and often found in guano and kidney stones [11,12]. Potentially advantageous properties of these MKPC binders include: near-neutral pH, low water demand, low drying shrinkage, and high early compressive strength [13–16].

$$MgO_{(s)} + KH_2PO_{4\,(s)} + 5H_2O_{(l)} \rightarrow MgKPO_4{\cdot}6H_2O_{(s)} \quad (1)$$

These cements have been proposed as a potential option for immobilisation of problematic radioactive waste streams occurring in the UK from more than 70 years of nuclear fuel operations. It is expected that these radioactive wastes will be treated by immobilisation and encapsulation techniques, and ultimately disposed of in a Geological Disposal Facility (GDF) after interim storage. The immobilisation of intermediate level waste (ILW) in suitable and stable wasteforms is a diverse and urgent challenge due to the high degree of variability in the physical/chemical composition and the waste condition (i.e. stored under water, inert gas, or open to air).

The current baseline option for immobilising ILW in the UK involves cementation using a composite of Portland cement (PC) blended with either fly ash (FA) or ground granulated blast furnace slag (BFS), to form FA/PC and BFS/PC grouts (with up to 75 wt% and 90 wt% replacements for PC, respectively) [17,18]. Portland cement composites are readily available, inexpensive and durable, and the PC grout preparation is straightforward in remote operations, and the Portland-based cement matrix imposes a high pH environment, which can assist in the immobilisation of many radionuclides (particularly actinides) through the formation of less soluble hydroxide species and sorption to mineral phases [19–21]. Despite these attributes, there is an increasing awareness that PC composites may not be suitable for the immobilisation/encapsulation of all ILW waste types present in the inventory [5,6,19], in particular reactive metal waste streams such as Magnox swarf derived from mechanically decanned Mg-alloy fuel cladding for Magnox

* Corresponding author.
E-mail address: n.c.hyatt@sheffield.ac.uk (N.C. Hyatt).

https://doi.org/10.1016/j.cemconres.2021.106375
Received 4 August 2020; Received in revised form 8 January 2021; Accepted 19 January 2021
Available online 4 February 2021

reactors, and metallic U-containing wastes.

The high pH of blended PC composites (≈pH 13) [22] promotes the corrosion of Al, whilst Mg and U metals are known to corrode in wet environments [5,23–26]. Corrosion of reactive metals is considered to be problematic on two grounds: (1) the formation of expansive corrosion products (e.g. $Mg(OH)_2$, UO_2) that can cause a volumetric change within the wasteform, leading to the formation of stress-induced fractures [27] and (2) formation of hydrogen gas, which presents a flammable hazard (during interim storage, transportation, and disposal). Both have the potential to result in pressurisation and distortion of the waste container [28]. Consequently, the durability of the monolithic wasteform and its ability to retain radioactivity can be deleteriously affected, alongside a risk to the GDF of flammable gas build-up. It is therefore desirable that the corrosion rate of encapsulated reactive metals is controlled to ensure that the waste packages remain within regulatory tolerance. For these reasons, there is a clear need to develop a toolbox of tailored encapsulation systems that are compatible with specific wastes. Some of the alternative cement binders under investigation as potential encapsulants for reactive metals (due to their lower pH and/or lower water content) include aluminosilicate geopolymer cements, calcium aluminate cement (CAC), calcium aluminium phosphate (CAP), calcium sulphoaluminate (CSA) and magnesium potassium phosphate cement (MKPC) [5,19]. For the case of MKPC, it is proposed that the lower water-to-solids (w/s) ratio of a MKPC grout (often ≤0.3 w/s, compared to typical PC blends at ≥0.3 w/s), combined with water being chemically bound within the struvite-K crystal structure, might reduce the availability of free water for metallic waste (Mg/Al alloy, U-metal fuel) corrosion.

The behaviour of MKPC encapsulating reactive metals has focused on metallic Al [5], grouting of a reactor with metallic Al components [7,29,30], Magnox swarf (Mg) metal encapsulation, U-metal pucks/discs [31,32], and U-metal containing sludges [25]. Corrosion trials of natural U-metal pucks within FA/MKPC binders prepared with 0.26 and 0.28 w/s ratio showed that corrosion and gas generation rates were significantly lower than FA/PC grout (3:1, 0.42 w/s) [31]. However, it is favourable to lower the water content of these cements even further to reduce corrosion. Based on the literature [33,34]; lowering the water content, if optimised correctly, should not be detrimental to the compressive strength, volume stability or fluidity.

In this study, we develop blended MKPC formulations with fly ash (FA) or blast furnace slag (BFS) with the aim of further reducing the w/s ratio, and hence reducing reactive metal corrosion, whilst maintaining a fluid grout with acceptable setting and strength characteristics for radioactive waste encapsulation. Since our previous research indicated that BFS is not inert within MKPC systems [35], we perform detailed characterisation of the reactivity of this phase by studying the early age hydration of the formulations, including in-situ synchrotron powder X-ray diffraction. Finally, the efficacy of the reduced water content MKPC blends to retard reactive U-metal corrosion was assessed during a 700-day corrosion experiment.

2. Experimental programme

2.1. Materials

The precursors used were MgO (RBH Ltd., 89% purity), in the form of dead burnt magnesia (DBM), KH_2PO_4 (Prayon, >99% purity) as E340 MKP and granular H_3BO_3 (Fisher Scientific, >99.5% purity). Fly ash (FA) was supplied by CEMEX (450-S grade, conforming to BS EN 450-1 [36]). Blast furnace slag (BFS) was supplied by Hanson Cements (from Scunthorpe works) in accordance with established Sellafield Limited BFS specification for use in the UK nuclear industry [18]. It is a blend of fine slag and coarse calumite of the similar chemical composition at a ratio of 2:1. Detailed characterisation of this slag blend is reported by Sanderson et al. [37,38]. The characterisation and chemical compositions of the precursors are noted in Tables 1 and 2. Particle size distribution (PSD) was determined using a Malvern Mastersizer 3000 laser diffraction particle size analyser, with powder fineness measured using a Controls 62-L0041/A Blaine fineness apparatus calibrated using NIST SRM material 114q. Brunauer-Emmett-Teller (BET) surface area measurements were carried out using a Coulter SA 3100 instrument, the density was determined using a Micromeritics AccuPyc II 1340 pycnometer, and the oxide compositions were determined using X-ray fluorescence (XRF) analysis (using a PANalytical PW2404 spectrometer with powder fused into lithium tetraborate beads).

Table 1
Characterisation of raw materials using PSD, Blaine fineness, and BET surface area.

Material	d_{10} (μm)	d_{50} (μm)	d_{90} (μm)	Blaine fineness (m^2/kg)	BET S.A. (m^2/kg)
MgO	3.2 ± 0.1	24.4 ± 0.3	63.8 ± 0.6	329 ± 16	563 ± 72
KH_2PO_4	250 ± 1.5	600 ± 4.9	1210 ± 16.5	n.d.	n.d.
FA	2.7 ± 0.1	14.0 ± 0.3	66.1 ± 3.5	560 ± 10	2258 ± 10
BFS	1.6 ± 0.1	16.0 ± 0.1	1465 ± 15	497 ± 17	993 ± 72

Table 2
Composition of raw materials determined by XRF analysis (precision ±0.1 wt%).

Compound (wt%)	MgO	FA	BFS
Na_2O	<0.1	1.1	0.4
MgO	88.9	1.7	7.9
Al_2O_3	1.7	25.2	12.0
SiO_2	4.3	50.2	36.6
P_2O_5	<0.1	0.3	<0.1
K_2O	0.1	3.6	0.7
CaO	2.1	2.4	40.2
Fe_2O_3	1.5	9.3	0.4
Total	98.8	93.8	98.3

2.2. Mix design

The blended MKPC formulations (Table 3) were based on a 1.7: 1 MgO: KH_2PO_4 molar ratio, which has been developed for nuclear applications by Covill et al., [6] and Gardner et al., [35], with w/s ratios (0.22, 0.24, and 0.26) calculated based on mass (g) where the w/s = H_2O/Σ(MgO, KH_2PO_4, H_3BO_3 and FA/BFS). FA and BFS were included in the formulation design as diluents, which were added in a quantity of 50% of the mass of reactive binder constituents, including the mix water but excluding H_3BO_3 (Table 3). H_3BO_3 was added as a set retarder, as 2 wt% of the cementitious components (MgO, $KHPO_4$ and H_2O). In addition, an MKPC-only binder (0.24 w/s) was produced to understand the impact of FA/BFS on the early age hydration behaviour in blended MKPC binders. The MgO:KH_2PO_4 (M/P) molar ratio and retarder addition were fixed to 1.7:1 and 2 wt%, respectively, commensurate with the formulations reported in Table 3. The formulation design for a 500 g MKPC-only (0.24 w/s) batch was: 132.1 g MgO, 262.3 g KH_2PO_4, 95.8 g H_2O and 9.8 g H_3BO_3.

The precursors were mixed initially for 10 min in a Kenwood benchtop mixer, added in the following order: H_2O, H_3BO_3, FA (or BFS), MgO, and KH_2PO_4. Afterwards, the paste was transferred to a high shear

Table 3
FA/MKPC and BFS/MKPC formulations based on three water-to-solids (w/s) ratios; 0.22, 0.24 and 0.26 w/s (±0.1 g precision).

w/s	MgO (g)	KH_2PO_4 (g)	H_2O (g)	FA or BFS (g)	H_3BO_3 (g)
0.22	160.0	318.0	180.0	329.0	13.0
0.24	156.0	309.0	193.0	329.0	13.0
0.26	149.0	303.0	206.0	329.0	13.0

Silverson mixer operating at 4000 rpm for 10 min to ensure that a homogenous paste was achieved. For compressive strength measurements, paste was cast into steel 50 mm cube moulds (lined with plastic film as MKPCs can bond to steel [39]) and cured in an environmental chamber at 20 °C and 95% relative humidity until testing. For analysis of fresh pastes (i.e. mini-slump and calorimetry analysis), small batches (<100 g) were prepared by hand; the pastes were mixed for 2 min prior to analysis to allow for very early age data to be collected.

2.3. Analysis methods

The physical properties of the blended MKPC binders were measured using the mini-slump technique on a sheet of poly(methylmethacrylate) marked with 2 × 2 cm grid squares. The cone was a poly(tetrafluoroethylene) cone based on a scaled-down Abrams cone: (h = 57 mm, d (top) = 19 mm and d (bottom) = 38 mm) [40]. A photograph was taken of the final slump from directly above the sample after 1 min, the slump area was then calculated using ImageJ software [41] calibrated to the grid squares. Each formulation was tested in triplicate using three separate batches per formulation (a total of nine measurements), similar to the methodology reported in [42]. The error bars are equivalent to 1 standard deviation. The average time between each triplicate test (allowing for resetting equipment) was ~2 min, with all measurements per batch were completed within ~8–10 min. Using this method, there was no significant spread of data observed within individual paste batches suggesting reliable and reproducible results were obtained. Calorimetry analysis was performed using an eight channel isothermal calorimeter (TAM Air, TA instruments) set at 20 °C. Each sample was mixed externally for 2 min (as described in Section 2.2), after which the homogenous paste was weighed into a plastic ampoule (~15 g) and placed in the instrument for 7 days.

Paste samples cured for 7 days were crushed and subsequently ground using an agate mortar and sieved to <63 μm prior to powder XRD analysis. This was undertaken using a STOE STADI P diffractometer with an image plate detector (Cu Kα, 1.5406 Å) with diffraction patterns collected between 10 and 50° 2θ. Thermogravimetric analysis (TGA) was conducted on samples cured for 28 days using a Pyris 1 TGA instrument in an aluminium crucible at a heating rate of 10 °C/min to 1000 °C in a nitrogen atmosphere. Compressive strength was determined from 50 (±0.50) mm cubes at 3, 7 and 28 days curing ages, using a Controls Automax 5.0 testing machine at a load rate of 0.25 MPa/s. The values reported correspond to an average of three measurements, with errors of ±1 standard deviation. Calorimetry was performed on all formulations using an isothermal calorimeter (TAM Air, TA Instruments) at 20 °C, with each sample (~15 g) weighed into a plastic ampoule and placed into the instrument for 7 days. Setting was determined by Vicat testing, using a Mastrad E040 automatic Vicat apparatus, with fresh cement poured into a 70 mm diameter mould on a Perspex plate. A 1.13 mm diameter needle in free-fall mode was used to penetrate the cement every 15 min.

To determine the early age reactions occurring in MKPC systems, time-resolved synchrotron powder X-ray diffraction (SXPD) was conducted on Beamline I11 at the Diamond Light Source on fresh blended MKPC pastes (0.24 w/s formulation only). The intense incident beam with a calibrated wavelength of λ = 0.82570(5) Å was used to measure diffraction patterns from the samples. In a disposable container, the H_3BO_3 was added to H_2O and stirred for 1 min, after which, the dry precursors (MgO, KH_2PO_4 and FA/BFS) were added and mixed for an additional 2 min. Using capillary action, the cement paste was drawn into Kapton® polyimide tubes ($d = 0.8$ mm) and was flame sealed inside a borosilicate capillary tube ($d = 1$ mm) prior to analysis using the position sensitive detector (PSD) and sample changing robot with scan times typically of 2 min, at intervals up to 60 h post-mixing. Detailed descriptions of the SXPD instrument and long-duration SXPD experiments can be found in [43,44].

2.4. Uranium corrosion experiment

Gas evolution was determined by measuring the gas displacement of water over time. Cement samples were cast into 15 mL centrifuge tubes, into which a strip of uranium-foil (Goodfellow, supplied as 0.178 mm thick foil, 99.98% purity) was placed. The U-foil was pre-cleaned with nitric acid, then rinsed in distilled water to remove any external oxide formation, and cut into 10 × 29 mm strips, with one strip placed into each fluid cement sample. Samples were prepared and set-up in triplicate for FA/MKPC and BFS/MKPC formulations (0.24 w/s) and in duplicate for the BFS/PC (3:1, 0.35 w/s) formulation, because only 8 experimental stations were available.

The cement samples were sealed into glass vessels with a single thin glass spout to allow gas escape but not water ingress. The vessels were each placed into 5 L glass beakers filled with water, with a water-filled upended measuring cylinder (with wide neck) clamped in place over the gas egress spout. A schematic diagram of the set-up is shown in Fig. 1. The water was periodically re-filled due to evaporation and treated with Virkon-S disinfectant to eliminate the risk of microbial growth. Gas formation was measured by visually determining the volume of water displaced from the measuring cylinder, with cylinders re-filled when nearly empty of water. This method likely over-stated hydrogen evolution due to de-gassing of the water, however, this set up does enable a quantitative assessment of gas evolution over a long timeframe between sample sets. For the duration of the experiment (700 days), the temperature was recorded hourly with a data logger and the average temperature was determined to be 22.5 ± 2.5 °C (±1 standard deviation). Additional U-foil containing samples were cast at the same time and stored under the same temperature regime to allow for destructive testing (sectioning for SEM-EDX analysis) at 18 months, without affecting the gas evolution experiment.

3. Results and discussion

3.1. Paste properties

Mini-slump measurements were conducted on all formulations to provide a measure of fluidity, which is important to ensure that the grout is pourable to allow for complete encapsulation of complex shapes often encountered in the immobilisation of nuclear waste. The mini-slump results (Fig. 2) revealed that the blended MKPC binders (except the 0.22 w/s FA/MKPC paste) achieved a flow area equivalent to, or greater than, the baseline Portland cement (PC) composite grout typically used

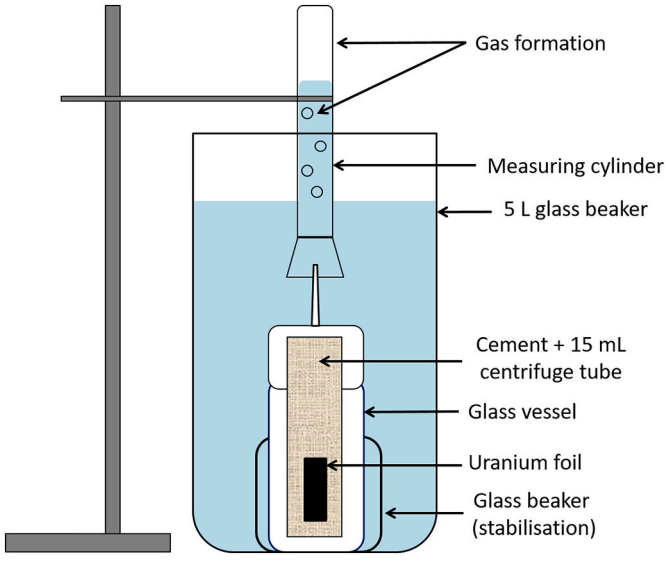

Fig. 1. Schematic of the experimental setup for one sample.

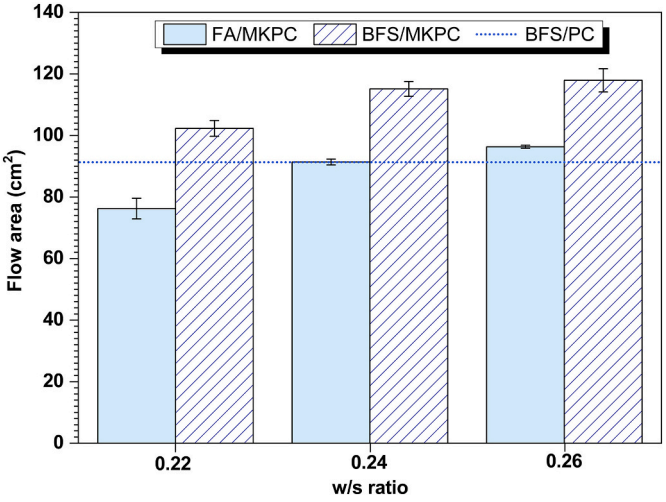

Fig. 2. Mini-slump flow areas of fresh FA/MKPC and BFS/MKPC pastes at 0.22, 0.24 and 0.26 w/s ratios compared to a BFS/PC grout (0.35 w/s) represented by the dashed line.

in the UK nuclear industry (91.3 ± 1.7 cm^2 with a 3:1 BFS/PC ratio, 0.35 w/s), with the miniature-slump flow area increasing commensurately with an increasing water content. The BFS/MKPC mixes consistently produced larger flow areas, which was unexpected as the inclusion of FA in MKPC binders was anticipated to enhance the workability (i.e. fluidity) more than the angular BFS particles as a result of the "ball-bearing effect" of the spherical FA particles [45–48]. The characteristics of the raw materials, however, help in part to explain the differences observed in mini-slump measurements. The FA used in this study had a finer particle size (resulting in a higher powder surface area) than BFS (Table 1), which is a special blend of fine/coarse material used for nuclear waste encapsulation in the UK. Consequently, it is expected that the FA absorbed more water than the BFS, leading to reduced overall fluidity of the FA/MKPC paste. Detailed powder properties for the blended fine/coarse BFS are reported in [38].

Only minor differences were observed between the flow areas of the 0.24 and 0.26 w/s ratios in the FA/MKPC and BFS/MKPC pastes: 5 cm^2 and 3 cm^2, respectively. By utilising the 0.24 w/s ratio formulation, there would be an 8% reduction in the water content without having a notable negative impact upon the workability designed for UK nuclear applications. Any reduction in the water content of the cement encapsulant would be expected to reduce the rates of reactive metal corrosion, as the presence of water is a driver for uranium corrosion [49]. The setting times of these blended binders was observed to increase commensurate with an increasing in w/s ratio (Table 4), which indicates that the FA/BFS diluted the precursors and delayed the acid-base reaction, leading to extended workability in addition to improved flow properties (Fig. 2). The initial and final set time for MKPC-only was suddenly achieved by 1.25 h; this highly exothermic reacion led to the samples being hot to touch. These results support the utilisation of diluents for applications of MKPCs where control of the setting time/workability are required (e.g. plant operations) and where strict heat generation limits exist (e.g. nuclear waste immobilisation). From Table 4, it was apparent that the blended BFS systems set more quickly than the FA containing cements despite being the most fluid samples, which infers a different mechanism between the two systems. The setting times observed for both the FA/MKPC and BFS/MKPC binders (Table 4) were close to the reported values for a similar formulation design, which ranged between 4.5 and 5 h (initial set) at 0.26–0.28 w/s with the final setting noted to be within 24 h [6].

Table 4
Setting time of MKPC formulations determined using Vicat measurements.

Sample	w/s	Initial set (h)	Final set (h)
MKPC only	0.24	1.25	1.25
FA/MKPC	0.22	2.0	6.0
FA/MKPC	0.24	4.5	7.0
FA/MKPC	0.26	5.0	7.5
BFS/MKPC	0.22	1.0	4.5
BFS/MKPC	0.24	2.0	6.0
BFS/MKPC	0.26	3.5	7.0

The compressive strength (CS) of blended MKPC binders was found to vary as a function of both the supplementary cementitious material used (FA, BFS) and the water content (Fig. 3). CS values for FA/MKPC binders reached between 20 and 25 MPa at 28 days of curing, which is comparable to literature values based on a similar system [6]. The 0.22 w/s FA/MKPC sample achieved the lowest strength, with a CS value of 19.93 ± 1.00 MPa at 28 days curing. Overall, the highest strengths were achieved by the 0.24 and 0.26 w/s FA/MKPC samples, which were within one standard deviation and close to the CS values achieved for an MKPC-only (0.24 w/s) formulation prepared using similar methods (previously published, achieving 14.71 ± 0.25 MPa, 18.82 ± 0.36 MPa and 22.65 ± 1.27 MPa at days 3, 7 and 28, respectively [35]).

The BFS/MKPC binders were observed to have superior mechanical properties compared to the FA/MKPC binders, with the CS values ranging between 25 and 36 MPa for the w/s ratios at 28 days of curing, with the highest strength achieved by the 0.22 w/s BFS/MKPC sample, in contrast to the FA/MKPC system. The difference in mechanical properties could in part be explained by FA, which has a smaller particle size (14.0 ± 0.3 μm, Table 1: d_{50}) and larger surface area (560 m^2/kg, Table 1: Blaine fineness) than BFS (16.0 ± 0.3 μm (d_{50}), 497 m^2/kg, Table 1). This results in FA having a greater water demand during the initial setting phase, which would reduce the amount of water available for struvite-K formation. Secondly, the difference could also be associated with the different particle packing capabilities of FA (spherical particles) and BFS (angular particles), where the latter has a better physical interlocking in the MKPC binder than FA [50], leading to improved mechanical performance.

Compared to other MKPC studies, the CS values reported for both the FA/MKPC and BFS/MKPC were on the lower range of achievable strength for MKPC systems. In the present study, the M/P molar ratio was fixed to 1.7:1. This M/P molar ratio is relatively low: values between 3:1 to 10:1 are typically used [13–15,51–54], resulting in CS values >40 MPa at 28 days curing [14,15,53]. Recent studies have indicated that the

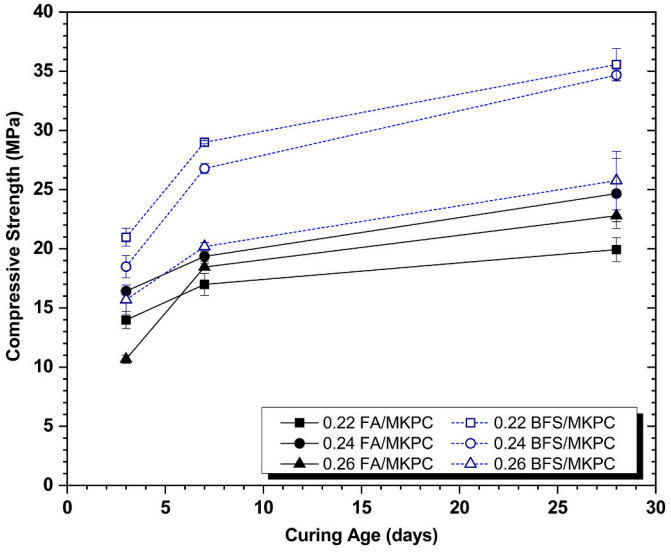

Fig. 3. Compressive strength of FA/MKPC and BFS/MKPC hardened pastes cured for up to 28 days, as a function of the w/s ratio (NB: the 0.24 w/s data set was previously included in [35]).

highest compressive strengths at w/s ratios ~0.2 are typically achieved when the M/P ratio is in the range of between 4:1 to 6:1 [13,33,34] with observed CS values in the range of ~60 MPa at 28 days. The compressive strength can decrease, by up to 40 MPa, when the M/P ratio is below 4 (at 0.2 w/c) in diluent-free systems [13]. Another parameter that may impact the strength development in the present study (compared to MKPC literature) is the inclusion of 50 wt% filler (FA/BFS), which effectively dilutes the total quantity of the cementitious binding phase (struvite-K), although much of the MgO bulk in higher M/P ratio systems (e.g. 6:1) does not react, acting largely as a filler once set.

In the present study, the formulation design stemmed from [5,6] with specific targets on the heat of hydration, fluidity and setting time for application within UK nuclear waste applications. In the UK, there is no set limit for compressive strength of cemented waste packages, the only requirement is for wasteforms to have "sufficient mechanical strength" for normal operations (storage, stacking, transportation) and accident scenarios (impact, fire) [55]. Therefore, the compressive strength values reported in Fig. 3 are likely to be appropriate for the target application, albeit lower than the potential mechanical properties achievable following formulation amendments.

3.2. Powder X-ray diffraction

The X-ray diffraction patterns of the 7-day cured FA/MKPC and BFS/MKPC binders are shown in Fig. 4. These binders do not form additional crystalline phases after further curing, data shown here correlate to those observed at 28 days of curing [35]. Diffuse scattering was identified between $15° < 2\theta < 25°$ and $25° < 2\theta < 35°$ in the FA/MKPC and BFS/MKPC binders, respectively, which is associated with the glassy fractions present in the fly ash (aluminosilicate) and slag (calcium aluminosilicate) precursors. Struvite-K ($MgKPO_4{\cdot}6H_2O$, powder diffraction file (PDF) #01-075-1076) was observed as the main crystalline phase, with traces of periclase (MgO, PDF #00-045-0946) identified in all formulations, which was added in excess (1.7:1 MgO:KH_2PO_4 molar ratio). This was to ensure that the KDP was fully consumed during the acid-base reaction and to provide nucleation sites for the formation of struvite-K [56,57]. In Fig. 4A, quartz (SiO_2, PDF #00-011-0252), mullite ($3Al_2O_32SiO_2$, PDF #00-015-0776) and hematite (Fe_2O_3, PDF #87-1164) from FA were identified, whilst åkermanite ($Ca_2MgSi_2O_7$, PDF #01-076-0841) reflections from BFS were observed in Fig. 4B.

The phase assemblage of the blended MKPC binders did not appear to change with the varying water content (w/s ratio). However, with an increased w/s ratio, the relative intensity of the struvite-K reflections increased commensurately with a decreased relative intensity of the main periclase reflection at $2\theta = 42.9°$. This was especially prevalent for the FA/MKPC system at 0.22 w/s ratio, which suggests a difference in the degree of reaction at lower w/s ratios. The results presented suggest that blended MKPC binders are chemically stable to small alterations in the water content and do not form additional crystalline phases due to reaction between MgO/KH_2PO_4 and the diluent material, forming only $MgKPO_4{\cdot}6H_2O$ as a crystalline material.

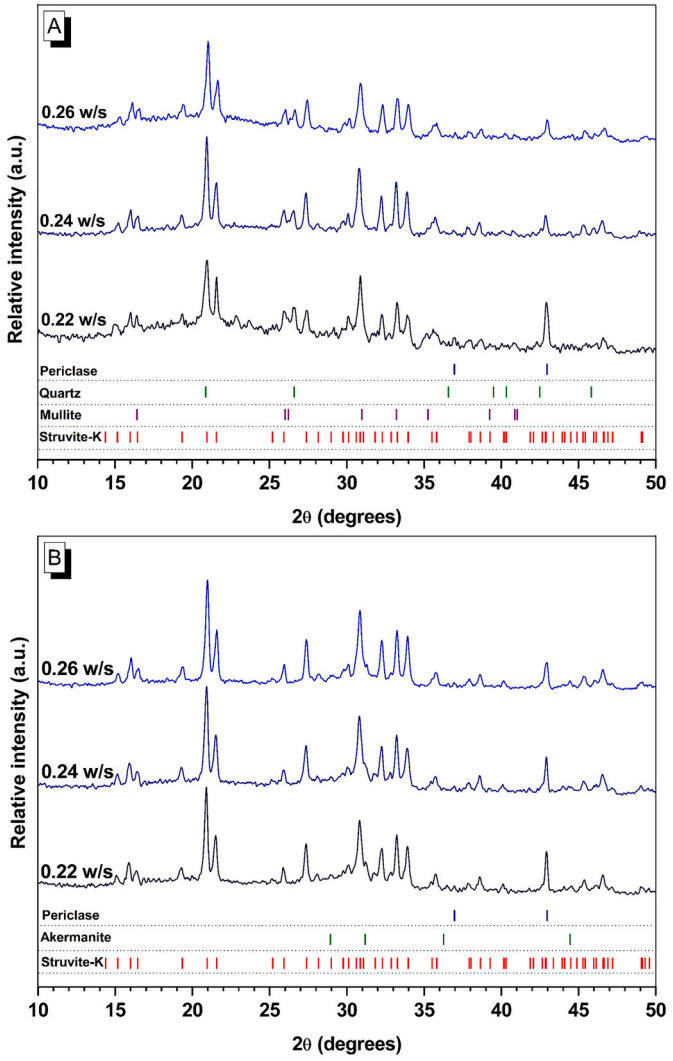

Fig. 4. X-ray diffraction patterns of A) FA/MKPC and B) BFS/MKPC pastes at various w/s ratios after 7 days of curing ($\lambda = 1.5406$ Å).

3.3. Thermal analysis

The dehydration behaviour of the blended MKPC binders (Figs. 5–6) revealed a single mass loss event between 50 and 150 °C (based on a 10 °C/min heating rate), associated with the one-step dehydration of $MgKPO_4{\cdot}6H_2O$ to $MgKPO_4$ (Eq. (2)), in agreement with literature using similar heating regimes [53,54,58]. In the FA/MKPC system, the mass losses observed up to 120 °C were: 17.0%, 17.8%, and 18.6% for w/s ratios 0.22, 0.24, and 0.26, respectively. In the BFS/MKPC system (Fig. 6), the mass losses were observed to be 14.1%, 16.3%, and 16.9% for w/s ratios 0.22, 0.24, and 0.26, respectively. This strongly suggests that the increased w/s ratio can result in an increased yield of struvite-K, though this needs to be balanced against the physical effects in fluidity, setting and strength. The assessments here, however, hold valid if only struvite-K is formed. No other crystalline phases were identified with XRD analysis, however we have previously reported evidence of an

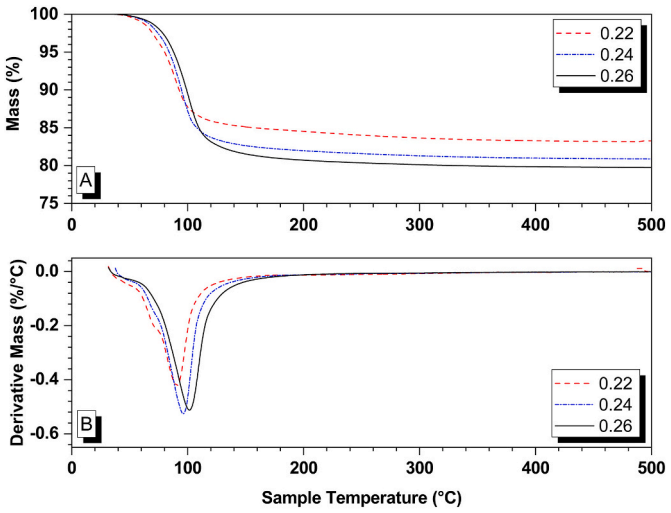

Fig. 5. TGA A) and DTG B) traces of hardened FA/MKPC pastes after 28 days of curing, at various w/s ratios.

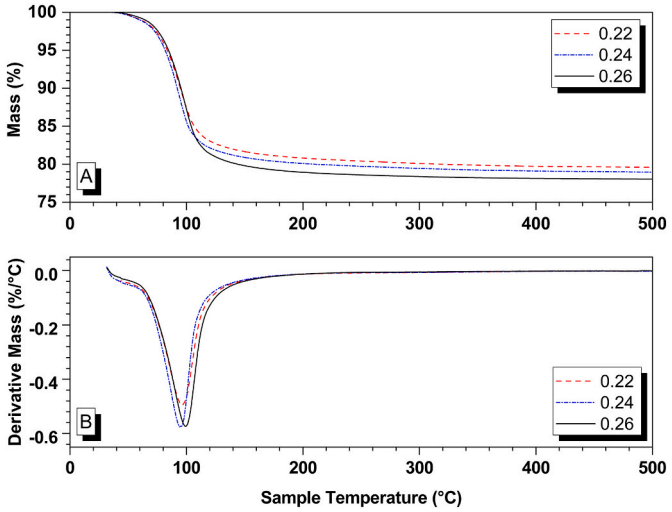

Fig. 6. TGA A) and DTG B) traces of hardened BFS/MKPC pastes after 28 days of curing, at various w/s ratios.

additional unknown reaction product within the BFS/MKPC system [35].

$$MgKPO_4{\cdot}6H_2O_{(s)} \rightarrow MgKPO_{4\ (s)} + \uparrow 6H_2O_{(g)} \quad (2)$$

3.4. Early age hydration behaviour from 0 to 60 h

To further study the effect of water content on the reaction of these systems, and whether the diluents (FA, BFS) might be reacting, isothermal calorimetry (IC) was conducted on the 0.22, 0.24 and 0.26 w/s formulations. In addition, time-resolved synchrotron XRD (SXPD) was undertaken on the 0.24 w/s formulation (as a mid-point in the water content) to provide high-resolution data about the early age setting reactions within the MKPC system. Both of these analyses were performed in conjunction with an MKPC-only (0.24 w/s) binder, which was used as a reference.

3.4.1. MKPC-only

In Fig. 7, the calorimetric traces of the MKPC-only binder (1.7:1 MgO:KH_2PO_4, 0.24 w/s, no diluent) show a a rapid exothermic peak, with the maximum exotherm achieved around ≈1 h. Closer inspection of the initial exotherm reveals some complexity, with a small endotherm at ~6 min, which is attributed to KH_2PO_4 dissolution (endothermic)

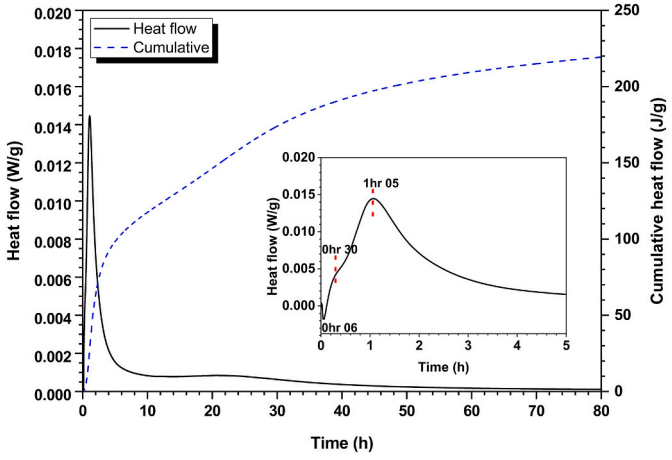

Fig. 7. Normalised calorimetric traces for MKPC-only at 0.24 w/s, with data for 0–5 h expanded in the inset.

[59,60]. In Fig. 7, there is a shoulder (~30 min) to the main exotherm, which is likely exothermic MgO dissolution, prior to the exothermic precipitation of struvite-K at 1 h 5 min, which was close to the setting time for the MKPC-only binder at 1 h 15 min (Table 4).

A second exothermic event occurred between 10 and 50 h, which was associated with a low heat generation. The early shape (<10 h) of the calorimetric trace of the MKPC-only sample is similar to that reported in the literature for conventional acid-base magnesium phosphate cements (with no diluent) [59,61], however, data are limited as most calorimetric studies for MKPC do not extend beyond 24 h. Qiao et al. [59] identified two exothermic peaks, associated with the dissolution of MgO in a weakly acidic media (caused by KH_2PO_4 dissolution), followed by the crystallisation of struvite-K [59]. However, this study extended only to 5.5 h (also using high M/P ratios of 2 to 11, resulting in rapid crystallisation) and so did not identify the later shallow exotherm observed here. Viani & Mácová reported calorimetry data up to 13 h [62] and suggested that the presence of the later exotherm was indicative of an amorphous product crystallising to struvite-K, though this has not been confirmed by other researchers. We interpret this shallow exotherm as the continuation of struvite-K formation from MgO reaction with phosphate in the pore solution, though kinetically limited by the formation of an interconnected struvite-K network, limiting Mg mobility.

3.4.2. FA/MKPC

The calorimetric traces for FA/MKPC pastes at w/s ratios 0.22, 0.24 and 0.26 are presented in Fig. 8. The hydration behaviour of the FA/MKPC binders appeared broadly comparable in heat flow to the MKPC-only binder (Fig. 7), though with three exothermic peaks detected. The first well-resolved and short exotherm likely corresponds to initial MgO dissolution, and potentially some dissolution of soluble alkalis from FA [63]. The second exotherm at ~2–5 h is associated with the precipitation of struvite-K, delayed compared to the MKPC-only paste in Fig. 7, with the third peak attributed to the continuous formation of struvite-K within a more restricted, hardened system. The position of each exotherm shifted to longer reaction times with an increased water content, with the third exotherm particularly drawn out up to ~70 h in the 0.26 w/s FA/MKPC sample. The delay in formation of struvite-K (peak 2) is commensurate with the delay in setting times in Table 4, observed with increasing water content.

The FA/MKPC binders had a lower thermal response during the dissolution/precipitation than the MKPC-only binder. This is expected as the FA/MKPC binders are diluted with 50 wt% FA, resulting in a lower exothermic output. In a previous study, the formation of a poorly crystalline potassium aluminosilicate was reported following a secondary reaction between the FA (or BFS) and MKPC components [35], however, there was no distinct isothermal calorimetry (IC) feature that could be assigned to this mechanism in the FA/MKPC binder and it is likely hidden by the high signal from the struvite-K formation reaction.

The hydration behaviour of the FA/MKPC binder (0.24 w/s ratio) was observed from 0.5 to ~60 h using synchrotron powder X-ray diffraction (SXPD) (Fig. 9). During the early time points (0.5–1.5 h), the only reflections in the diffraction patterns were those associated with unreacted periclase (MgO, PDF #00-045-0946) and the crystalline phases present in the FA: mullite (PDF #00-015-0776), quartz (SiO_2, PDF #00-011-0252) and hematite (Fe_2O_3, PDF #00-087-1164). The emergence of struvite-K ($MgKPO_4{\cdot}6H_2O$, PDF #01-075-1076) reflections was observed at 2 h, after which the relative intensity of these reflections increased (up to 60 h) commensurate with periclase consumption. This is in agreement with the IC data (Fig. 8) where the precipitation was estimated to begin by 2 h of curing and a weak exotherm was observed, extending to 70 h, and attributed to continued struvite-K formation.

Prior to the crystallisation of struvite-K at 2 h, neither the phosphate reagent (KDP) nor intermediate phosphate phases were identified in the FA/MKPC binder. This indicated that the complete dissolution of KDP

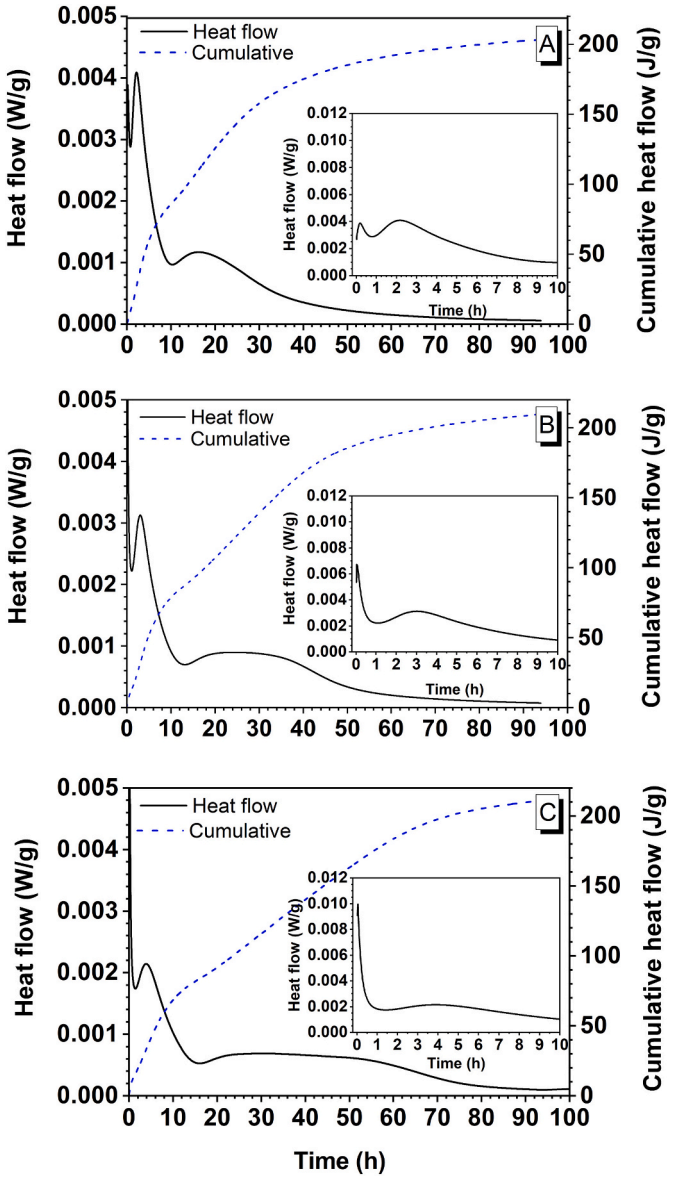

Fig. 8. Normalised calorimetric traces for fresh FA/MKPC pastes at A) 0.22 w/s, B) 0.24 w/s and C) 0.26 w/s, with data for 0–10 h expanded in the inset in each plot.

occurred between the sample preparation and prior to the first diffraction pattern being collected at 30 min. To highlight this, the KDP (PDF#00-035-0807) was included in Fig. 9. Due to the narrow Kapton tubes (ø = 0.8 mm), the KDP was ground slightly using a pestle and mortar to reduce the particle size, which may have increased the reactivity of the KDP compared to the calorimetry samples (although this does not appear to have affected struvite-K formation times). Crystalline phases reported here are in agreement with the results of Viani et al. using both 1.7:1 and 1:1 Mg:P ratios [62,64].

The early hydration behaviour by SXPD of the FA/MKPC binder does not reveal the formation of any crystalline phase other than struvite-K. Therefore, no additional crystalline phases can account for the later exotherm in Fig. 8 (10–60 h), which must be either attributed to the continued formation of struvite-K (also consistent with consumption of MgO) or the formation of a poorly crystalline product. The latter cannot be comprehensively proven in this study but recent literature proposes the presence of poorly crystalline phases within MKPCs as: 1) an intermediate product in MKPCs with no diluents [62] and 2) a secondary reaction product from MKPC – FA interactions [35].

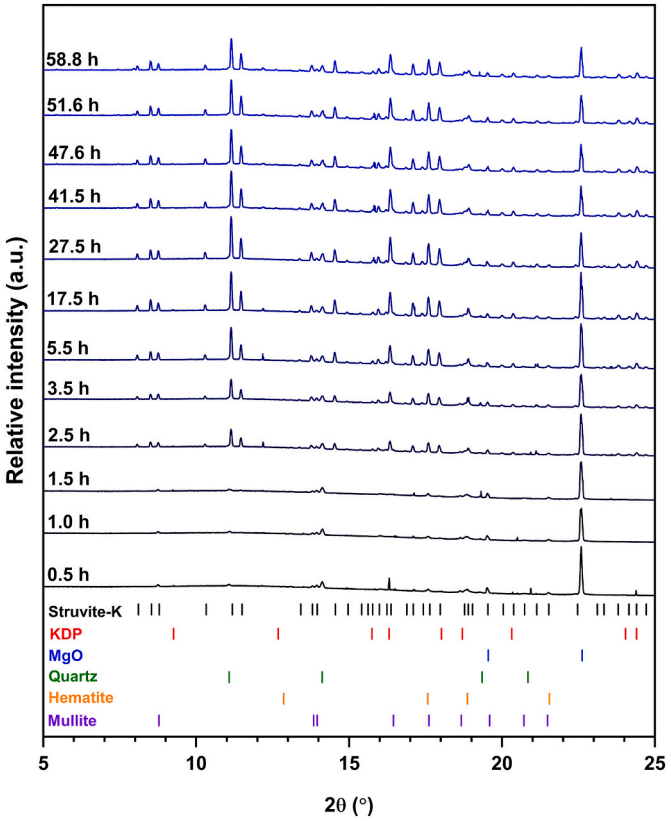

Fig. 9. Time-resolved SXPD patterns of 0.24 w/s FA/MKPC binder up to 58.8 h (λ = 0.82570 Å).

Lahalle et al. [60,65] reported that the early age hydration of MKPCs could lead to the formation of various additional magnesium phosphate phases such as $MgHPO_4{\cdot}7H_2O$, $Mg_2KH(PO_4)_2{\cdot}15H_2O$, or $Mg_3(PO_4)_2{\cdot}22H_2O$, which were stable throughout the duration of their ex-situ hydration experiments. However, there was no evidence to support the formation of such phases in this in-situ hydration experiment, shown in Fig. 9. Those ex-situ studies utilised high w/s ratios (100 [60] and 1 [65]) to elucidate a mechanistic understanding of MKPC hydration as opposed to this study, where formulations were designed for UK nuclear waste applications (e.g. lower water content, 0.24 w/s) as such, direct comparisons should not be drawn.

3.4.3. BFS/MKPC

The calorimetric traces of the BFS/MKPC binders at 0.22, 0.24 and 0.26 w/s ratios (Fig. 10) reveal a considerable difference in the hydration behaviour compared to both the MKPC-only and FA/MKPC binders. Within the BFS/MKPC binders an initial well-resolved exotherm (<1 h) was observed, potentially associated with MgO dissolution (Fig. 10 inset). This was followed by an induction period (with low but not zero signal), which increased consummately with an increased water content, for example, the delay was ~8 h for 0.22 w/s and ~20 h at 0.26 w/s. Following the induction stage, an exotherm was observed with three distinct, but overlapping peaks, increasingly delayed with higher contents of water. The 0.26 w/s sample, in particular, exhibited a long induction period with low (though not zero) heat output, before the first heat output peak at ~45 h. This implies the presence of altered reaction kinetics in the BFS/MKPC binders compared to the FA/MKPC binders.

The reactivity of the BFS might explain the early setting characteristics of the BFS/MKPC blends, since BFS is known to at least partially react in these systems [35]. All the BFS samples have a faster initial and final set, compared to the FA samples, despite delayed exothermic reactions. Within the FA samples, the setting times are roughly

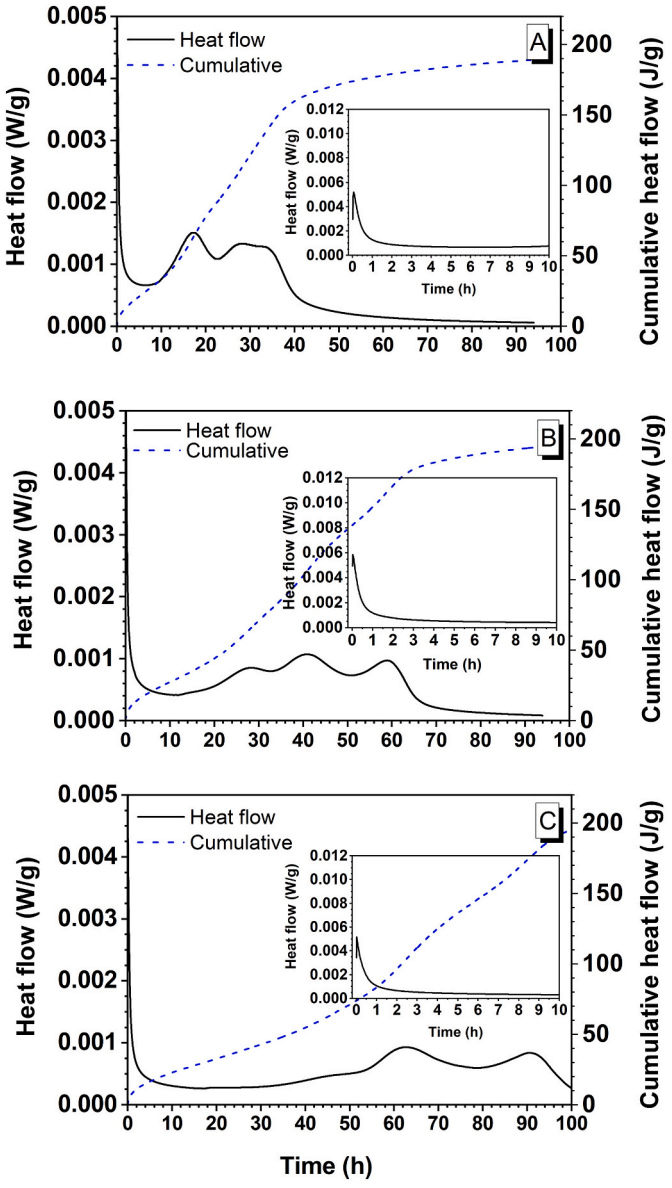

Fig. 10. Normalised calorimetric traces for fresh BFS/MKPC pastes at A) 0.22 w/s, B) 0.24 w/s and C) 0.26 w/s, with data for 0–10 h expanded in the inset in each plot.

commensurate with the observed exothermic reactions in Fig. 8, whilst with BFS, setting appears delayed with respect to the thermal response (Fig. 10). If, as with the FA samples, the exothermic features represent struvite-K crystallisation, this implies the formation of an intermediate product in BFS/MKPC which contributes at least to early stiffening of the cement paste (as the final set was observed between 4.5 and 7 h) (Table 4).

The time-resolved in-situ SXPD data of the 0.24 w/s BFS/MKPC binder (Fig. 11) support the occurrence of a delayed reaction mechanism, concurring with the calorimetry data (Fig. 10). In the first two hours post-mixing, only reflections associated with MgO and KDP were detected, in contrast to the FA/MKPC binder at a similar time point (Fig. 9) where KDP had fully reacted.

The SXPD data show evidence of preferred orientation, especially for the KH_2PO_4 (KDP) reflections. The stronger (200) and (321) reflections at 12.73° and 24.05° 2θ respectively were greatly reduced by 2.2 h. This does not indicate KDP dissolution, as the major (112) reflection at 2θ = 16.32° increased in relative intensity, along with other minor

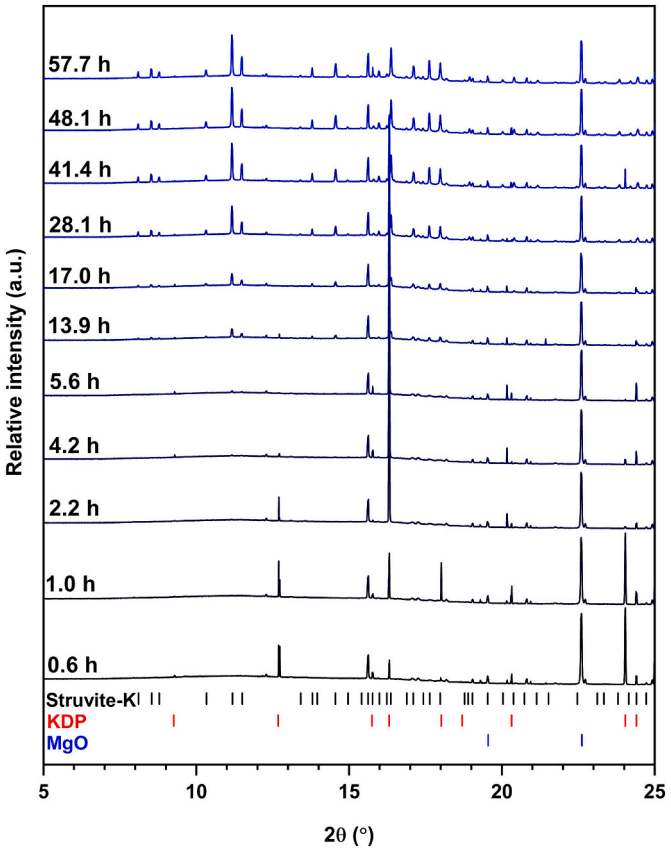

Fig. 11. Time-resolved SXPD patterns of 0.24 w/s BFS/MKPC binder up to 58.8 h (λ = 0.82570 Å).

reflections. No other phases could accurately be matched to these reflections, leading us to infer preferential KDP orientation due to the large crystallite size and confinement of the small capillary tube. This is evidenced by the lack of struvite-K reflections until 13.9 h, at which time the major KDP reflection at 2θ = 16.32° begins to decrease in relative intensity (more noticeable over a smaller 2θ range in Fig. 12), with KDP reflections disappearing by 57.7 h, in line with the emergence of struvite-K reflections.

The formation kinetics of struvite-K observed by SXPD agree well with the calorimetry data in Fig. 10, where an exothermic reaction occurred at ~12 h, exactly when struvite-K formation was observed to initiate. The first exothermic peak maximum, associated with struvite-K formation, occurred at ~25 h, which was in agreement with SXPD where the relative intensities of struvite-K reflections were observed to increase (28.1 h scan, Fig. 11). This struvite-K crystallisation occurs after the cement sets, further suggesting evidence of an intermediate product, which is poorly crystalline in nature, as no other crystalline products were observed prior to 13.9 h. However, other poorly crystalline features are present in this synchrotron data from both the BFS and the Kapton capillary, so we are unable to confirm its presence due to these complicating background signals.

3.5. Formulation design summary

The main motivation for the present study was to modify the MKPC formulation design with specific reference to UK specific requirements for cement encapsulation of radioactive waste. Previous work (UK) reported formulations between 0.26 and 0.32 w/s at M/P molar ratio 1.5:1, which utilised 50 wt% FA as a diluent (for cost savings and to reduce heat of hydration) and 2 wt% boric acid (set retarder) for improved workability [5,6,66]. It is within these specific requirements

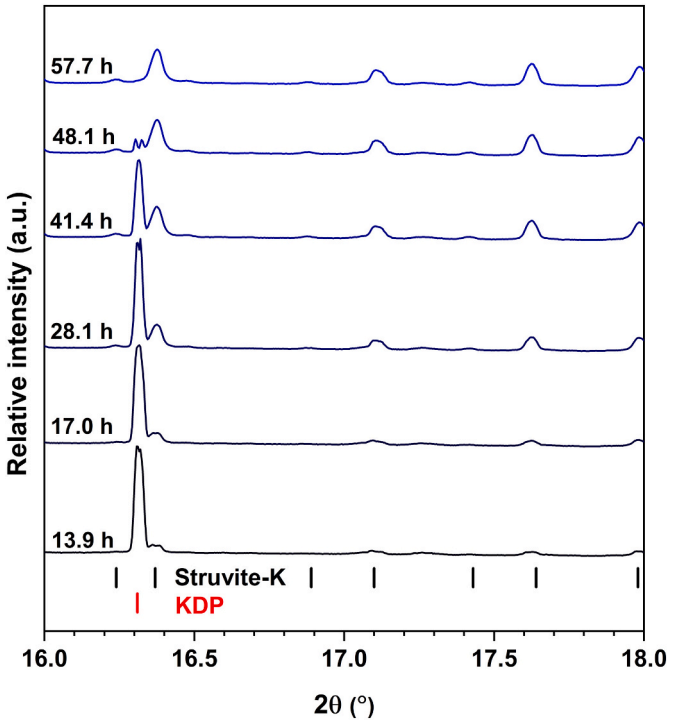

Fig. 12. Time resolved SXPD patterns of 0.24 w/s BFS/MKPC binder between $16° \leq 2\theta \leq 18°$, from 13.9–57.7 h ($\lambda = 0.82570$ Å).

and targeted application (reactive metal encapsulation) that we define our "optimised" w/s ratio. In the lowest w/s ratio (0.22 w/s), the fluidity of the FA/MKPC binder was below the current UK nuclear industry standard grout (BFS/OPC) and both FA/BFS systems had the quickest initial and final set times (Table 4). The rapid setting and lower water content of the 0.22 w/s binder appeared to affect the total quantity of struvite-K formed in these systems, as evidenced by the increased relative intensity of the main MgO reflection at $2\theta = 42.8°$ (indicating more unreacted MgO; Fig. 4) and the smaller mass loss at ~100 °C (associated with struvite-K dehydration; Fig. 5). The MKPC formulation design allows for unreacted MgO, which provides nucleation sites for struvite-K crystallisation. However, excessive MgO could be problematic if it undergoes a delayed hydration reaction (to form $Mg(OH)_2$), which is associated with a volume increase and could affect wasteform integrity (e.g. stress-induced cracking). Therefore, the 0.22 w/s formulation was deemed not suitable for further investigation.

To differentiate between the 0.24 and 0.26 w/s formulations, the results indicated that no significant improvement could be identified based on the phase assemblage, fluidity or compressive strength. The setting times were slightly longer at 0.26 w/s, whilst the compressive strength was higher (albeit within one standard deviation) at 0.24 w/s. The fluidity revealed that both FA/MKPC and BFS/MKPC binders matched or exceeded the reported values for BFS/OPC suggesting that both water contents could maintain workability during plant operations. Therefore, the "optimised" formulation must be derived from the overall water content required to decrease the corrosion rate of encapsulated reactive metals arising from intermediate level waste streams in the UK. The 0.24 w/s formulation appeared to be the most suitable, and as such, was content chosen for metallic uranium corrosion trials (Section 3.6).

However, it should be noted that the calorimetry data for the BFS/MKPC formulations were dissimilar from the MKPC-only, FA/MKPC and reported literature for these systems. Our in-situ SPXD studies revealed that the 0.24 w/s BFS/MKPC binder achieved the same end point (formation of a single hydrated phosphate phase) but the utilisation of BFS impacted the setting reaction, struvite-K crystallisation timeframe (Fig. 11) and extended/lowered the reaction heat output (Fig. 10). These blended MKPC formulations warrant further investigation to explore, in detail, the different reaction kinetics between the FA/MKPC and BFS/MKPC binders.

3.6. Interaction between MKPC binders and reactive uranium metal

To determine the performance of the optimised blended MKPC formulation for nuclear waste management applications, particularly targeting reactive metals, a small-scale encapsulation experiment was performed using uranium metal, and monitored up to day 700 post-mixing. The aim of this experiment was to measure gas evolution from both FA and BFS blended MKPC (0.24 w/s) samples, compared with a conventional BFS/PC blend (3:1 blend, 0.35 w/s). The oxidative corrosion of U metal by water yields hydrogen, according to Eq. (3), therefore the total gas evolution can be used as a means to quantify the extent of corrosion, although this is not an absolute measure of corrosion. The generation of uranium hydride, according to Eqs. (4) and (5), is a particular concern as it is unstable in air and pyrophoric in specific conditions (e.g. high surface area), which generates challenges associated with the management and disposal of metallic uranium wastes [49,67,68].

$$U_{(s)} + 2H_2O_{(l)} \rightarrow UO_{2\ (s)} + 2H_{2\ (g)} \quad (3)$$

$$U_{(s)} + 1.5H_{2\ (g)} \rightarrow UH_{3\ (s)} \quad (4)$$

$$UH_{3\ (s)} + 2H_2O_{(l)} \rightarrow UO_{2\ (s)} + 3.5H_{2\ (g)} \quad (5)$$

The cumulative gas evolution (with minimum, mean and maximum values) for the all three binder systems are presented in Fig. 13. It was immediately apparent that the gas evolution from the FA/MKPC and BFS/MKPC formulations were significantly lower than that for BFS/PC. The averaged cumulative gas evolution after 700 days was calculated to be: 64.7 ± 15.0 mL, 70.4 ± 12.7 mL and 143.5 ± 2.7 mL (±1 standard deviation), for FA/MKPC, BFS/MKPC and BFS/PC, respectively. From these values, little difference could be assigned between the behaviour of the two blended MKPC binders. Fig. 13 highlights the importance of conducting long-term corrosion studies to underpin the corrosion behaviour of the encapsulating grout and waste. Below 50 days, the difference in gas evolution between all binder systems was almost within one standard deviation (indicating similar corrosion behaviour). However, above 200 days, a clear divergence in the gas evolution rate was

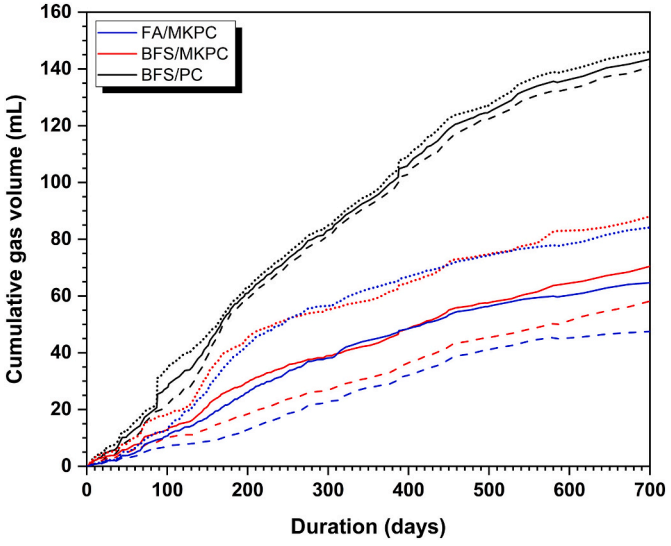

Fig. 13. Cumulative gas evolution for uranium encapsulated within FA/MKPC, BFS/MKPC and BFS/PC binders, up to day 700 (the solid line represents the mean value, the dotted line represents the minimum value and the dashed line represents the maximum value).

observed, indicative of an improved wasteform performance for the blended MKPCs due to a lower overall gas evolution (which infers a lower uranium corrosion rate than BFS/PC, within the remit of this experiment).

To explore the corrosion behaviour further, gas evolution rates (determined by linear regression) are reported in Table 5 for three time ranges: 0–200 days, 200–450 days and 450–700 days. The time periods were identified based on observed changes in the BFS/PC trace in Fig. 13. For all formulations, the highest evolution rate occurred between the first 200 days after which, the rate of gas evolution slowed between 200 and 450 days and further between 450 and 700 days. The final evolution rate (450–700 days), revealed that FA/MKPC and BFS/MKPC gas evolution rates, at 0.044 ± 0.001 mL d^{-1} and 0.062 ± 0.001 mL d^{-1} respectively, were an order of magnitude lower than that for the BFS/PC system (0.102 ± 0.005 mL d^{-1}). Given that U-metal corrosion is dominated by aqueous oxidation to UO_2, it is clear that the blended MKPC formulations confer reduced reactivity due to the lower proportion of free water.

Comparison with other U corrosion studies is challenging due to differences in experimental protocols, and there are fewer studies that include an MKPC binder. At the Pacific Northwest National Laboratory (USA), a magnesium phosphate cement, Tectonite (a proprietary formulation) was found to have a higher hydrogen generation from encapsulated metallic uranium beads when compared to a range of PC-based grouts [25]. This was dissimilar to the results of Covill [31], who reported that FA/MKPC grouts (0.26 and 0.28 w/s) performed considerably better than a FA/PC grout (3:1, 0.42 w/s) encapsulating natural U pucks. Since there was no information given about the composition of the Tectonite material, an explanation for why the present study shows the opposite result is not apparent, but it may be due to the greater surface area of the U metal beads, when compared to natural U pucks (~20 cm^2) [31] and the metallic U strips (~5.9 cm^2) used in the present study.

Overall the results of the present study indicate that the employment of blended MKPC binders in the encapsulation of metallic U has the potential to reduce reactive metal corrosion by half, when compared to a UK nuclear industry standard grout, BFS/PC. Furthermore, a continued drive towards lower water content could further improve performance, although corrosion will still proceed, albeit at a low rate.

At 18 months, sacrificial samples were taken for microstructural analysis using SEM-EDX, with one sample for FA/MKPC and BFS/MKPC. Unfortunately, corrosion within the BFS/PC sample had caused substantial cracking, and the sample broke apart during sectioning. As such it is not possible to demonstrate the U-cement interaction for BFS/PC for comparison with the FA/MKPC and BFS/MKPC samples (Fig. 14). Further work is planned to investigate the effect of uranium corrosion on these binders, including using non-destructive techniques.

The backscattered electron micrographs of the FA/MKPC and BFS/MKPC binders encapsulating U-foil were typical for magnesium phosphate binders. In the FA/MKPC binder (Fig. 14A), large struvite-K crystallites, unreacted periclase and the spherical particles associated with fly ash were clearly evident. A good adhesion with the U-foil (which appears as bright white contrast) was observed with only minor indication of uranium corrosion, as further evidenced by enhanced magnification of the foil-cement interface in Fig. 15. No apparent cement/uranium interactions could be observed at the magnification presented in Fig. 14A. The elemental maps suggest that K and Ca (Fig. 14A: K and Ca) were associated with the uranium foil, however this is due to an overlap of the characteristic X-rays detected by EDX analysis and the overall low Ca content (2.4 wt% in FA, Table 2), which resulted in a background signal across the sample. For K, the strong $K\alpha_1$ X-ray at 3.314 keV (used in Fig. 14) coincided with the $M\beta_1$ X-ray of U at 3.336 keV. Attempts were made to isolate the K signal from U by using the $K\beta_1$ emission at 3.590 keV with narrow windowing. However, the resulting signal was weak, which resulted in K being detected uniformly across the microstructure even in particles with no K (e.g. fly ash and slag particles), due to background signal in this region. Therefore, K cannot be differentiated from U due to signal overlaps, but the U foil is clearly distinguishable from the cement matrix.

The SEM/EDX data for the BFS/MKPC sample are quite different, with a continuous struvite-K matrix observed, embedded with angular BFS particles. The condition of the encapsulated U-foil displayed clear corrosion on all exposed surfaces (Fig. 14B), with the corrosion layer spalling away from the metal, creating a gap between the MKPC binder and the U-foil. This is indicative of the formation of UO_2 in a porous laminar layer, which is reported to spall in sheets from the underlying metal surface [49]. No other elements appeared to be associated with the U corrosion layer other than U (noting the K, U energy overlap as for the FA/MKPC binder), further implying that it is composed only of UO_2.

The clear difference in corrosion between the BFS/MKPC and FA/MKPC samples does not concur with the long-term gas evolution studies. The BFS/MKPC system continually released more gas than the FA/MKPC system however, the averaged cumulative values at day 700 were within one standard deviation of each other. This may suggest that localised regions of high corrosion may persist, which were not fully captured in the analysis if the sacrificial sample for FA/MKPC, or that there might be differences in the metal-cement interface between samples, for example the shrinkage of cement paste allowing room for spalling to occur.

Table 5
Gas evolution rates from FA/MKPC, BFS/MKPC and BFS/PC binders (using the mean data depicted in Fig. 14).

Binder	Evolution rate (mL d^{-1})		
	Day 0–200	Day 200–450	Day 450–700
FA/MKPC	0.129 ± 0.002	0.106 ± 0.001	0.044 ± 0.001
BFS/MKPC	0.145 ± 0.002	0.091 ± 0.001	0.062 ± 0.001
BFS/PC	0.312 ± 0.001	0.224 ± 0.001	0.102 ± 0.005

4. Conclusions

MKPC formulations blended with FA and BFS with a w/s ratio ranging from 0.22–0.26, were developed and characterised with the aim to maintain key physical properties, such as setting time, fluidity and compressive strength for potential deployment as a radioactive waste encapsulant. Detailed analysis of the hydration behaviour of these blends was investigated, with calorimetry data and time-resolved SXPD revealing significant differences in the early reaction behaviour, reaction commencement and duration between MKPC blended with FA and BFS. SXPD revealed that in FA/MKPC and BFS/MKPC binders (at a M/P molar ratio of 1.7:1), struvite-K was the only observed crystalline hydration product. Notably, the addition of BFS to the system delayed the crystallisation of struvite-K by ~14 h in the 0.24 w/s system, in contrast to only ~2 h in the FA/MKPC system. The setting of the BFS/MKPC system was observed prior to formation of crystalline struvite-K, which suggests the formation of an intermediate poorly crystalline product, whereas the setting and crystallisation of FA/MKPC were broadly in agreement with the diluent-free MKPC system. The delayed setting of BFS/MKPC may be advantageous for industrial applications (especially larger products / wasteforms) as the thermal output and setting time can be controlled by modifying the diluent added to the MKPC binder. The optimised blended MKPC binders (0.24 w/s ratio) in this study were found to reduce the corrosion of uranium by up to 50% when compared to the UK nuclear grout (3:1 BFS/PC) for cementation and, as such, offer a promising alternative for immobilising radioactive metal inventories, as well as for use in other applications that involve close contact of cement with reactive metals.

CRediT authorship contribution statement

Laura J. Gardner: Methodology, Formal analysis, Investigation, Writing – Original Draft, Visualization.

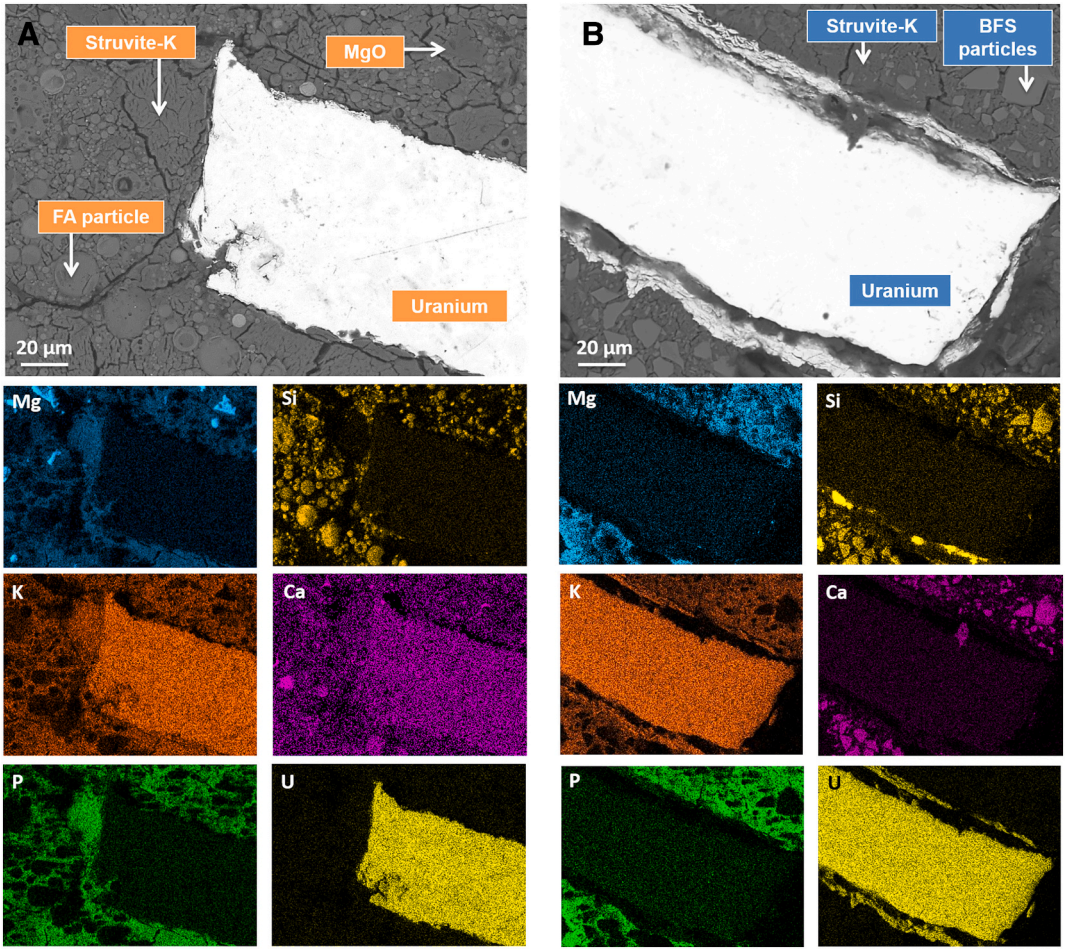

Fig. 14. A) FA/MKPC (0.24 w/s) with encapsulated uranium foil at 18 months, B) BFS/MKPC (0.24 w/s) with encapsulated uranium foil at 18 months.

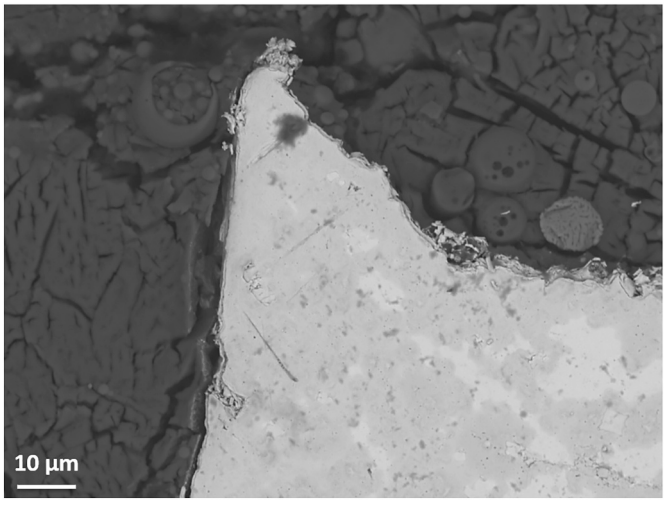

Fig. 15. BSE micrograph of FA-MKPC sample at higher magnification.

Claire L. Corkhill: Conceptualization, Methodology, Investigation, Writing – Review & Editing.

Sam A. Walling: Investigation, Formal analysis, Writing – Review & Editing.

James E. Vigor: Investigation, Formal analysis, Writing – Review & Editing.

Claire A. Murray: Methodology, Investigation, Writing – Review & Editing.

Chiu C. Tang: Methodology, Investigation, Writing – Review & Editing.

John L. Provis: Investigation, Writing – Review & Editing, Supervision.

Neil C. Hyatt: Conceptualization, Methodology, Investigation, Writing – Review & Editing, Supervision, Funding acquisition.

Declaration of competing interest

The authors declare that they have no known competing financial interests or personal relationships that could have appeared to influence the work reported in this paper.

Acknowledgements

LJG is grateful to the Nuclear Decommissioning Authority (NDA) for sponsorship, under assistance by the National Nuclear Laboratory. NCH wishes to acknowledge the Royal Academy of Engineering and the Nuclear Decommissioning Authority for funding and EPSRC for part support under grant references EP/S032959/1, EP/P013600/1, and EP/N017617/1. CLC is grateful to the University of Sheffield for the award of a Vice Chancellor's fellowship and EPSRC for the award of an Early Career Fellowship under grant reference EP/N017374/1. We thank Diamond Light Source for access to beamline I11 (proposal number EE10038-1) that contributed to the results presented here. This research utilised the HADES/MIDAS facility at the University of Sheffield established with financial support from EPSRC and BEIS, under grant EP/T011424/1 [69].

References

[1] S.S. Seehra, S. Gupta, S. Kumar, Rapid setting magnesium phosphate cement for quick repair of concrete pavements — characterisation and durability aspects, Cem. Concr. Res. 23 (1993) 254–266.
[2] F. Qiao, C.K. Chau, Z. Li, Property evaluation of magnesium phosphate cement mortar as patch repair material, Constr. Build. Mater. 24 (2010) 695–700.
[3] G. Mestres, F.S. Aguilera, N. Manzanares, S. Sauro, R. Osorio, M. Toledano, M. P. Ginebra, Magnesium phosphate cements for endodontic applications with improved long-term sealing ability, Int. Endod. J. 47 (2014) 127–139.
[4] A.S. Wagh, R. Strain, S.Y. Jeong, D. Reed, T. Krause, D. Singh, Stabilization of Rocky Flats Pu-contaminated ash within chemically bonded phosphate ceramics, J. Nucl. Mater. 265 (1999) 295–307.
[5] M. Hayes, I.H. Godfrey, Development of the use of alternative cements for the treatment of intermediate level waste, in: WM'07 Conference Proceedings, AZ, USA, 2007, p. 7328.
[6] A. Covill, N.C. Hyatt, J. Hill, N.C. Collier, Development of magnesium phosphate cements for encapsulation of radioactive waste, Adv. Appl. Ceram. 110 (2011) 151–156.
[7] C. Cau Dit Coumes, D. Lambertin, H. Lahalle, P. Antonucci, C. Cannes, S. Delpech, Selection of a mineral binder with potentialities for the stabilization/solidification of aluminum metal, J. Nucl. Mater. 453 (2014) 31–40.
[8] A.S. Wagh, S.Y. Sayenko, V.A. Shkuropatenko, R.V. Tarasov, M.P. Dykiy, Y. O. Svitlychniy, V.D. Virych, E.A. Ulybkina, Experimental study on cesium immobilization in struvite structures, J. Hazard. Mater. 302 (2016) 241–249.
[9] Z. Lai, H. Wang, Y. Hu, T. Yan, Z. Lu, S. Lv, H. Zhang, Rapid solidification of highly loaded high-level liquid wastes with magnesium phosphate cement, Ceram. Int. 45 (2019) 5050–5057.
[10] M. Mathew, L.W. Schroeder, Crystal structure of a struvite analogue, $MgKPO_4{\cdot}6H_2O$, Acta Crystallogr. B Struct. Crystallogr. Cryst. Chem. 35 (1979) 11–13.
[11] E. Banks, R. Chianelli, R. Korenstein, Crystal chemistry of struvite analogs of the type $MgMPO_4{\cdot}6H_2O$ ($M^+ = K^+$, Rb^+, Cs^+, Tl^+, NH_4^+), Inorg. Chem. 14 (1975) 1634–1639.
[12] D.A. Hall, R. Stevens, B.E. Jazairi, Effect of water content on the structure and mechanical properties of magnesia-phosphate cement mortar, J. Am. Ceram. Soc. 81 (1998) 1550–1556.
[13] M. Le Rouzic, T. Chaussadent, L. Stefan, M. Saillio, On the influence of Mg/P ratio on the properties and durability of magnesium potassium phosphate cement pastes, Cem. Concr. Res. 96 (2017) 27–41.
[14] Y. Li, T. Shi, J. Li, Effects of fly ash and quartz sand on water-resistance and salt-resistance of magnesium phosphate cement, Constr. Build. Mater. 105 (2016) 384–390.
[15] S. Hong, J. Zhang, H. Liang, J. Xiao, C. Huang, G. Wang, H. Hu, Y. Liu, Y. Xu, F. Xing, B. Dong, Investigation on early hydration features of magnesium potassium phosphate cementitious material with the electrodeless resistivity method, Cem. Concr. Compos. 90 (2018) 235–240.
[16] S.A. Walling, J.L. Provis, Magnesia based cements – a journey of 150 years, and cements for the future? Chem. Rev. 116 (2016) 4170–4204.
[17] B. Batchelor, Overview of waste stabilization with cement, Waste Manag. 26 (2006) 689–698.
[18] Radioactive Waste Management, RWM HAW Innovation and Delivery: a review of cement powders secruity of supply, specifications and disposability issues, in: NDA Report No. NDA/RWM/144, Geological Disposal, 2016.
[19] N.B. Milestone, Reactions in cement encapsulated nuclear wastes: need for toolbox of different cement types, Adv. Appl. Ceram. 105 (2006) 13–20.
[20] J.H. Sharp, N.B. Milestone, J. Hill, E.W. Miller, Cementitious systems for encapsulation of intermediate level waste, in: The 9th International Conference on Radioactive Waste Management and Environmental Remediation Oxford, UK, 2003.
[21] N.D.M. Evans, Binding mechanisms of radionuclides to cement, Cem. Concr. Res. 38 (2008) 543–553.
[22] A. Vollpracht, B. Lothenbach, R. Snellings, J. Haufe, The pore solution of blended cements: a review, Mater. Struct. 49 (2016) 3341–3367.
[23] A. Setiadi, N.B. Milestone, J. Hill, M. Hayes, Corrosion of aluminium and magnesium in BFS composite cements, Adv. Appl. Ceram. 105 (2006) 191–196.
[24] A.R. Hoch, N.R. Smart, J.D. Wilson, B. Reddy, A Survey of Reactive Metal Corrosion Data for Use in SMOGG Gas Generation Model, Serco Ltd, Harwell, UK, 2010.
[25] C.H. Delegard, A.J. Schmidt, R.L. Sell, S.I. Sinnkov, S.A. Bryan, S.R. Gano, B. M. Thornton, Final Report: Gas Generation Testing of Uranium Metal in Simulated K Basin Sludge and in Grouted Sludge Waste Forms, PNNL, WA, USA, 2004.
[26] C.A. Stitt, C. Paraskevoulakos, A. Banos, N.J. Harker, K.R. Hallam, H. Pullin, A. Davenport, S. Street, T.B. Scott, In-situ, time resolved monitoring of uranium in BFS:OPC grout. Part 2: corrosion in water, Sci. Rep. 8 (2018) 9282.
[27] C. Paraskevoulakos, C.A. Stitt, K.R. Hallam, A. Banos, M. Leal Olloqui, C.P. Jones, G. Griffiths, A.M. Adamska, J. Jowsey, T.B. Scott, Monitoring the degradation of nuclear waste packages induced by interior metallic corrosion using synchrotron X-ray tomography, Constr. Build. Mater. 215 (2019) 90–103.
[28] Nuclear Decommissioning Authority, Geological Disposal: Gas Status Report NDA/RWMD/037, 2010.
[29] C. Langton, D.B. Stefanko, M.G. Serranto, J.K. Blankenship, W.B. Griffin, J. T. Waymer, D. Matheny, D. Singh, Use of cementitious materials for SRS reactor facility in-situ decommissioning, in: WM 2011 Conference, Phoenix, AZ, 2011, p. 11620.
[30] D.B. Stefanko, C.A. Langton, D. Singh, Magnesium Mono Potassium Phosphate Grout for P-reactor Vessel In-situ Decommissioning. SRNL-STI-2010-00333. Revision 0, ANL, IL, USA, 2010.
[31] A. Covill, Novel Encapsulants for Intermediate Level Waste in the UK Nuclear Industry, Ph.D. Thesis, Department of Materials Science and Engineering, University of Sheffield, 2010.
[32] W.J. Montague, The Suitability of Magnesium Phosphate Cemet for Uranium Metal Encapsulation, Ph.D. Thesis, Department of Materials, Imperial College London, London, UK, 2014.
[33] H. Ma, B. Xu, J. Liu, H. Pei, Z. Li, Effects of water content, magnesia-to-phosphate molar ratio and age on pore structure, strength and permeability of magnesium potassium phosphate cement paste, Mater. Des. 64 (2014) 497–502.
[34] H. Ma, B. Xu, Potential to design magnesium potassium phosphate cement paste based on an optimal magnesia-to-phosphate ratio, Mater. Des. 118 (2017) 81–88.
[35] L.J. Gardner, S.A. Bernal, S.A. Walling, C.L. Corkhill, J.L. Provis, N.C. Hyatt, Characterisation of magnesium potassium phosphate cements blended with fly ash and blast furnace slag, Cem. Concr. Res. 74 (2015) 78–87.
[36] British Standard, Fly Ash for Concrete. Part 1: Definition, Specifications and Conformity Criteria, BS EN 450-1, 2012.
[37] R.A. Sanderson, G.M. Cann, J.L. Provis, Comparison of calorimetric methods for the assessment of slag cement hydration, Adv. Appl. Ceram. 116 (2017) 186–192.
[38] R.A. Sanderson, G.M. Cann, J.L. Provis, The effect of blast-furnace slag particle size on the hydration of slag–Portland cement grouts at elevated temperatures, Adv. Cem. Res. 30 (2018) 337–344.
[39] S.E. Mouring, P.H. Miller, V.L. Burns, Investigation into the mechanical behaviour of ceramicrete, in: Proceedings of 13th International Offshore and Polar Engineering Conference, HI, USA, 2003.
[40] D.L. Kantro, Influence of water-reducing admixtures on properties of cement paste - a miniature slump test, Cem. Concr. Aggr. 2 (1980) 95–102.
[41] W.S. Rasband, ImageJ, U.S. National Institute of Health, Bethesda, Maryland, USA, 1997–2012.
[42] Z. Tan, S.A. Bernal, J.L. Provis, Reproducible mini-slump test procedure for measuring the yield stress of cementitious pastes, Mater. Struct. 50 (2017) 235.
[43] S.P. Thompson, J.E. Parker, J. Marchal, J. Potter, A. Birt, F. Yuan, R.D. Fearn, A. R. Lennie, S.R. Street, C.C. Tang, Fast X-ray powder diffraction on I11 at Diamond, J. Synchrotron Radiat. 18 (2011) 637–648.
[44] C.A. Murray, J. Potter, S.J. Day, A.R. Baker, S.P. Thompson, J. Kelly, C.G. Morris, S. Yang, C.C. Tang, New synchrotron powder diffraction facility for long-duration experiments, J. Appl. Crystallogr. 50 (2017) 172–183.
[45] R. Lewis, L. Sear, P. Wainwright, R. Ryle, Cementitious additions, in: J. Newman, B. Choo (Eds.), Advanced Concrete Technology: Constituent Materials Butterworth-Heinemann, UK, Oxford, 2003.
[46] Q. Yang, X. Wu, Factors influencing properties of phosphate cement-based binder for rapid repair of concrete, Cem. Concr. Res. 29 (1999) 389–396.
[47] Q. Yang, B. Zhu, X. Wu, Characteristics and durability test of magnesium phosphate cement-based material for rapid repair of concrete, Mater. Struct. 33 (2000) 229–234.
[48] Z. Liu, G. Qian, J. Zhou, C. Li, Y. Xu, Z. Qin, Improvement of ground granulated blast furnace slag on stabilization/solidification of simulated mercury-doped wastes in chemically bonded phosphate ceramics, J. Hazard. Mater. 157 (2008) 146–153.
[49] B.A. Hilton, Review of oxidation rates of DOE spent nuclear fuel, in: Part 1: Metallic Fuel. ANL-00/24, ANL, IL, USA, 2000.
[50] J.L. Provis, P. Duxson, J.S.J. van Deventer, The role of particle technology in developing sustainable construction materials, Adv. Powder Technol. 21 (2010) 2–7.
[51] A.-j. Wang, Z.-l. Yuan, J. Zhang, L.-t. Liu, J.-m. Li, Z. Liu, Effect of raw material ratios on the compressive strength of magnesium potassium phosphate chemically bonded ceramics, Mater. Sci. Eng. C 33 (2013) 5058–5063.
[52] A.-j. Wang, J. Zhang, J.-m. Li, A.-b. Ma, L.-t. Liu, Effect of liquid-to-solid ratios on the properties of magnesium phosphate chemically bonded ceramics, Mater. Sci. Eng. C 33 (2013) 2508–2512.
[53] L. Chong, J. Yang, C. Shi, Effect of curing regime on water resistance of magnesium–potassium phosphate cement, Constr. Build. Mater. 151 (2017) 43–51.
[54] L. Mo, L. Lv, M. Deng, J. Qian, Influence of fly ash and metakaolin on the microstructure and compressive strength of magnesium potassium phosphate cement waste, Cem. Concr. Res. 111 (2018) 116–129.
[55] Radioactive Waste Management, Geological Disposal: Guidance on the Production of Encapsulated Wasteforms. WPS/502/01, 2015, pp. 1–77.
[56] E. Soudée, J. Péra, Mechanism of setting reaction in magnesia-phosphate cements, Cem. Concr. Res. 30 (2000) 315–321.
[57] A.S. Wagh, S.Y. Jeong, Chemically bonded phosphate ceramics: I, a dissolution model of formation, J. Am. Ceram. Soc. 86 (2003) 1838–1844.
[58] L.J. Gardner, S.A. Walling, S.M. Lawson, S. Sun, S.A. Bernal, C.L. Corkhill, J. L. Provis, D.C. Apperley, D. Iuga, J.V. Hanna, N.C. Hyatt, Characterization of and structural insight into struvite-K, $MgKPO_4{\cdot}6H_2O$, an analogue of struvite, Inorg. Chem. 60 (2021) 195–205.
[59] F. Qiao, C. Chau, Z. Li, Calorimetric study of magnesium potassium phosphate cement, Mater. Struct. 45 (2012) 447–456.
[60] H. Lahalle, C. Cau Dit Coumes, A. Mesbah, D. Lambertin, C. Cannes, S. Delpech, S. Gauffinet, Investigation of magnesium phosphate cement hydration in diluted suspension and its retardation by boric acid, Cem. Concr. Res. 87 (2016) 77–86.
[61] D.A. Hall, R. Stevens, B. El-Jazairi, The effect of retarders on the microstructure and mechanical properties of magnesia–phosphate cement mortar, Cem. Concr. Res. 31 (2001) 455–465.

[62] A. Viani, P. Mácová, Polyamorphism and frustrated crystallization in the acid–base reaction of magnesium potassium phosphate cements, CrystEngComm 20 (2018) 4600–4613.
[63] A.G. Kim, G. Kazonich, M. Dahlberg, Relative solubility of cations in Class F fly ash, Environ. Sci. Technol. 37 (2003) 4507–4511.
[64] A. Viani, M. Peréz-Estébanez, S. Pollastri, A.F. Gualtieri, In situ synchrotron powder diffraction study of the setting reaction kinetics of magnesium-potassium phosphate cements, Cem. Concr. Res. 79 (2016) 344–352.
[65] H. Lahalle, C. Cau Dit Coumes, C. Mercier, D. Lambertin, C. Cannes, S. Delpech, S. Gauffinet, Influence of the w/c ratio on the hydration process of a magnesium phosphate cement and on its retardation by boric acid, Cem. Concr. Res. 109 (2018) 159–174.
[66] W. Montague, M. Hayes, L.J. Vandeperre, Strength - formulations correlations in magnesium phosphate cements for nuclear waste encapsulation, in: H.-T. Lin, Y. Katoh, A. Vomiero (Eds.), The American Ceramic Society's 37th International Conference on Advanced Ceramics and Composites FL, USA, 2014, pp. 107–117.
[67] A. Banos, K.R. Hallam, T.B. Scott, Corrosion of uranium in liquid water under contained conditions with a headspace deuterium overpressure. Part 2: the ternary $U + H_2O_{(l)} + D_2$ system, Corros. Sci. 152 (2019) 261–270.
[68] A. Banos, K.R. Hallam, T.B. Scott, Corrosion of uranium in liquid water under vacuum contained conditions. Part 1: the initial binary $U + H_2O_{(l)}$ system, Corros. Sci. 152 (2019) 249–260.
[69] N.C. Hyatt, C.L. Corkhill, M.C. Stennett, R.J. Hand, L.J. Gardner, C.L. Thorpe, The HADES facility for high activity decommissioning engineering & science: part of the UK national nuclear user facility, in: IOP Conference Proceedings: Materials Science and Engineering vol. 818, 2020 (012022).